ISSN 0023-1584, Kinetics and Catalysis, 2007, Vol. 48, No. 5, pp. 742–748. © MAIK "Nauka/Interperiodica" (Russia), 2007.
Original Russian Text © G.A. Zenkovets, A.A. Shutilov, V.Yu. Gavrilov, S.V. Tsybulya, G.N. Kryukova, 2007, published in Kinetika i Kataliz, 2007, Vol. 48, No. 5, pp. 792–799.

Formation of the Structure of Cerium Oxide–Modified Titanium Dioxide

G. A. Zenkovets, A. A. Shutilov, V. Yu. Gavrilov, S. V. Tsybulya, and G. N. Kryukova

Boreskov Institute of Catalysis, Siberian Branch, Russian Academy of Sciences, Novosibirsk, 630090 Russia

e-mail: Gavrilov@catalysis.nsk.su

Received April 5, 2006

Abstract—The formation of the structure of titanium dioxide containing 3–15 wt % CeO_2 in a wide temperature range (300–850°C) has been investigated by X-ray powder diffraction, electron microscopy, and adsorption methods. Modification of titanium dioxide with cerium oxide causes the formation of nanostructured Ce–Ti–O compounds consisting of incoherently intergrown fine anatase crystallites. The crystallites are separated by interblock boundaries in which cerium ions are stabilized. The nanostructure formed in the Ce–TiO_2 oxide system stabilizes the anatase phase, prevents the sintering of anatase particles at high temperatures, and allows modified anatase to retain a larger specific surface area and a higher porosity upon heat treatment than pure titanium dioxide does.

DOI: 10.1134/S0023158407050205

Anatase titanium dioxide is among the most common supports for various heterogeneous catalysts. Furthermore, anatase itself is used as a catalyst in acid–base catalysis and photooxidation [1–6]. It was demonstrated that the microstructure of titanium dioxide depends strongly on the preparation method [7–9]. Using different preparation methods, one can obtain microstructures ranging from highly ordered (regular) to defective. The structure of TiO_2 is strongly correlated with the physicochemical properties and texture of the oxide, which govern the interaction between the active component and the support. This unique possibility of purposefully modifying the structural properties of titanium dioxide is still attracting researchers' attention.

An efficient way of varying the structural properties of anatase, including its texture, is by modifying it with various cations, for example, vanadium [10], molybdenum [11, 12], and phosphorus [13]. The effect of a modifier on the TiO_2 structure depends on the chemical nature of the modifier. Modification of TiO_2 with vanadium or molybdenum affords a nanostructured material having interblock boundaries between anatase crystallites. As a result, this material is thermally more stable than the initial anatase. Furthermore, its smaller particle size and its larger specific surface area persist up to higher temperatures [10–12]. However, titanium dioxide modified with both molybdenum and vanadium is thermally less stable than pure TiO_2.

Introducing refractory modifiers, such as cerium dioxide, is likely to enhance the thermal stability of TiO_2. This would be significant for the synthesis of titanium dioxide–based supports and catalysts for high-temperature processes. Cerium–titanium oxides are used as supports in CuO/Ce–TiO_2 catalysts for the oxidation of CO, ethanol, and ethyl acetate [14] and for NO + CO reduction [15]; in supported metal catalysts for low-temperature CO oxidation [16]; and in photooxidation reactions [17]. In any case, the structure and physicochemical properties of the cerium–titanium oxide support are of primary importance in the formation of the active component.

It was shown that, as a mixture of cerium and titanium dioxides is heat-treated in an oxidizing atmosphere, the components do not react up to 1300°C, yielding no solid solutions or compounds [18–20]. However, the metastable compound $CeTi_2O_6$ with a monoclinic structure is detected at 1310–1350°C. As the temperature is further raised, this compound decomposes. Heat-treating a mixture of prereduced cerium and titanium oxides at T = 1200–1250°C and a reduced oxygen partial pressure yields a number of metastable variable-composition cerium–titanium compounds, namely, Ce_2TiO_5, $Ce_2Ti_2O_7$, $Ce_4Ti_9O_{24}$ [21], $CeTi_2O_{5.6}$, $CeTi_3O_{8.7}$, $CeTiO_3$ [19], $Ce_{0.75}TiO_{2.995}$, and $Ce_{0.90}TiO_{3.03}$ [22], which are unstable in air.

At the same time, it was demonstrated that cerium–titanium compounds can be synthesized not only at high temperatures, but also at comparatively low temperatures of 400–650°C [23–25]. For example, the monoclinic compound $Ce_{0.3}Ti_{0.7}O_2$ and a cubic solid solution of titanium in cerium dioxide were obtained by mixing an organometallic compound of titanium with cerium nitrate followed by drying and heat treatment of the mixture at 650°C [23]. $CeTiO_3$ with a perovskite structure was obtained by reacting an organometallic compound of titanium with cerium chloride at room temperature [24]; however, the product became amorphous above 400°C. Cerium–titanium compounds

Table 1. Heat-induced changes in the phase composition of the Ce–Ti–O materials

Chemical composition, wt %	*T*, °C			
	300	500	700	850
TiO_2	Anatase	Anatase	Anatase	Rutile
3% CeO_2	″	″	″	Anatase
5% CeO_2	″	″	″	Anatase + CeO_2 traces
10% CeO_2	″	″	Anatase + CeO_2 traces	Anatase + CeO_2
15% CeO_2	″	″	Anatase + CeO_2 traces	Anatase + CeO_2
CeO_2	CeO_2	CeO_2	CeO_2	CeO_2

(Ti/Ce = 4 : 1 and 1 : 1) stable at 800°C were obtained by sol–gel processing followed by redox reactions [25].

It follows from the above data that none of the Ce–Ti–O compounds has been found to retain the original anatase structure. However, as was mentioned above, it is anatase that is used in most catalysts.

Here, we report the formation of the structure of cerium-doped titanium dioxide (anatase) in a wide temperature range.

EXPERIMENTAL

Ce–Ti–O samples containing 3–15 wt % CeO_2 and 85–97 wt % TiO_2 were synthesized by incipient-wetness impregnation of anatase xerogels (0.5–1.0 mm size fraction) with an aqueous solution of $Ce(NO_3)_3 \cdot 6H_2O$ (reagent grade) followed by drying at 110°C for 10–12 h and heat treatment in flowing air at 300–850°C for 4 h.

The cerium content of the products was determined by ICP–AES.

Electron microscopic examinations were performed using a JEM 2010 microscope with a resolution of 1.4 Å and an accelerating voltage of 200 kV. The microscope was equipped with an EDAX energy-dispersive spectrometer, which allowed elemental analysis to be carried out.

The odorous structure of xerogels was studied by the conventional low-temperature (77.4 K) nitrogen adsorption method using a DigiSorb-2600 instrument (Micromeritics). True density (ρ, g/cm^3) was measured with an AutoPycnometer-1320 helium picnometer (Micromeritics). The total pore volume (V_Σ, cm^3/g) and porosity (ε, cm^3/cm^3) were derived from the bulk density (δ, g/cm^3) and true density using the conventional relationships $V_\Sigma = (0.6/\delta - 1/\rho)$ and $\varepsilon = V_\Sigma\rho/(1 + V_\Sigma\rho)$. The limiting sorption volume (V_s, cm^3/g), which is the microporous plus mesoporous part of the pore volume, was determined directly from adsorption data. The total specific surface area (S_{BET}, m^2/g) was derived from Ar thermal desorption data (four sorption equilibrium points) obtained using an SORBI-M instrument. The mean particle size of materials (d_{ads}, nm) was estimated as $d_{ads} = 6/S\rho$. The equivalent pore throat size distribution was derived from the desorption branches of nitrogen adsorption isotherms using the Barret–Joyner–Hallenda (BJH) method [26]. The dominant pore size (D_{dom}, nm) was indicated by a peak in the distribution curve.

The phase composition of materials was determined by X-ray powder diffraction (URD-63 diffractometer, monochromated CuK_α radiation). The coherent-scattering domain (CSD) size (d_{CSD}, nm) for anatase crystallites was derived from the halfwidth of the 2.0.0 peak using the Scherrer formula [27].

RESULTS AND DISCUSSION

The data presented in Table 1 show how the phase composition of the materials examined changes upon heat treatment. In the sample with a low cerium content (3 wt % CeO_2 + 97 wt % TiO_2), only the anatase phase is detected up to 850°C. Raising the cerium content to 10–15 wt % CeO_2 results in the formation of traces of CeO_2 at a lower temperature of 700°C. At the same time, the thermal decomposition of cerium nitrate yields well-crystallized CeO_2 at 300°C.

The microstructure and morphology of the Ce–Ti–O materials were studied by electron microscopy. It was demonstrated in an earlier work [7] that the initial titanium dioxide consists of aggregates of fine anatase particles 3–8 nm in size. These aggregates are combined into larger aggregates 70–90 nm in size. Titanium dioxide modified with cerium oxide has the same structure and morphology. Figure 1 shows an electron micrograph of the 15 wt % CeO_2 + 85 wt % TiO_2 catalyst calcined at 350°C. This micrograph is typical of the TiO_2–CeO_2 catalysts calcined at this temperature. It is clear that this sample consists of aggregates of 3- to 8-nm fine particles. According to electron microdiffraction data, the sample does not contain any appreciable amount of the CeO_2 phase. The electron microdiffraction pattern is a set of ring-shaped reflections indicating interplanar spacing characteristic of the anatase phase (Fig. 1). At the same time, elemental analysis data suggest the presence of cerium in the samples. Apparently, the modifying cerium on the surface of the anatase particles is in a near-atomic state of dispersion.

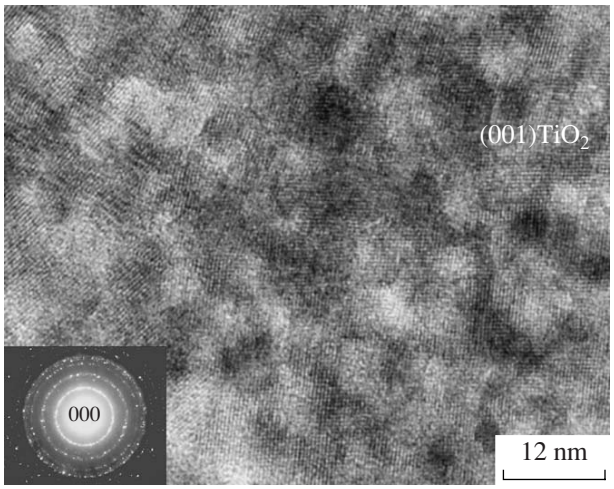

Fig. 1. Micrograph of the Ce–Ti–O sample containing 15% CeO_2. T_{calcin} = 350°C. Inset: the microdiffraction pattern characteristic of anatase titanium dioxide.

Note that, in all samples calcined at 350–600°C, no cerium oxide phase was detected by X-ray diffraction or electron microdiffraction and the unit cell parameters of the anatase phase are equal to those of pure anatase. However, the presence of cerium is indicated by microprobe analysis. Since anatase, CeO_2, and Ce_2O_3 have different structures and the ionic radii of Ce^{4+} and Ce^{3+} (0.88 and 1.02 Å, respectively) far exceed the ionic radius of Ti^{4+} (0.64 Å) [28], the cerium ions cannot be stabilized in the anatase lattice. This result is in full agreement with the finding that, in an oxidizing atmosphere, cerium and titanium oxides react only above 1300°C [18–20]. These data apparently suggest that, in the samples calcined at 600°C, most of the cerium ions are localized at interblock boundaries formed by anatase particle intergrowths, where the anatase structure is heavily disordered. Microprobe analysis data indicate that the signal from the Ce atoms strengthens as the accelerating voltage is reduced from 200 to 100 kV (Fig. 2). Since the probing depth in EDX analysis decreases as the accelerating voltage is reduced, the strengthening of the Ce signal possibly indicates that most of the cerium is localized near the surface.

Heat treatment of the Ce–Ti–O materials above 800°C causes the sintering of TiO_2 particles into crystals up to 50 nm in size and the transfer of cerium oxide from the interblock boundaries to the surface. It is clear from Fig. 3 that cerium leaves the interblock boundaries to concentrate as the cerium oxide phase. The alternating contrast bands in the image of the cerium oxide structure on the anatase surface are due to the overlapping of particles of two crystalline phases having different structures, namely, tetragonal TiO_2 and cubic CeO_2. Furthermore, anatase retains its block structure. Therefore, part of the cerium can remain at the interblock boundaries (see arrows). Apparently some cerium stays in the subsurface layer: the anatase surface has numerous steps with a distorted structure, and no cerium oxide crystallites are detectable on these steps (Fig. 4). Cerium ions can also be present at intercrystal boundaries (which are noted by arrows in Fig. 4).

The electron microscopic data are in agreement with our X-ray diffraction data (Fig. 5). It follows from the latter that all samples calcined at 850°C consist only of the anatase phase and contain no rutile traces, irrespective of the cerium content. Traces of the cerium oxide

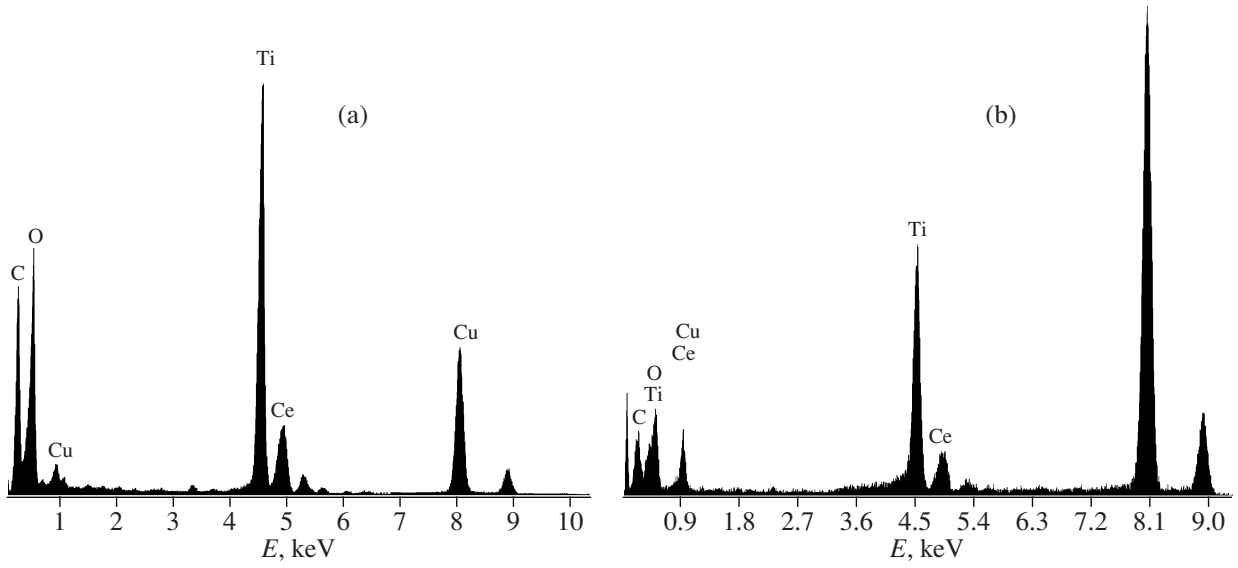

Fig. 2. EDX microanalysis data for the Ce–Ti–O sample containing 15% CeO_2. T_{calcin} = 600°C. The accelerating voltage is (a) 200 and (b) 100 kV.

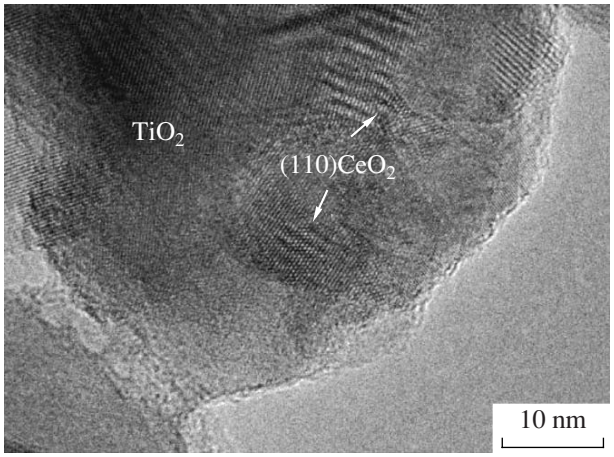

Fig. 3. Micrograph of the Ce–Ti–O sample containing 5% CeO_2. T_{calcin} = 850°C

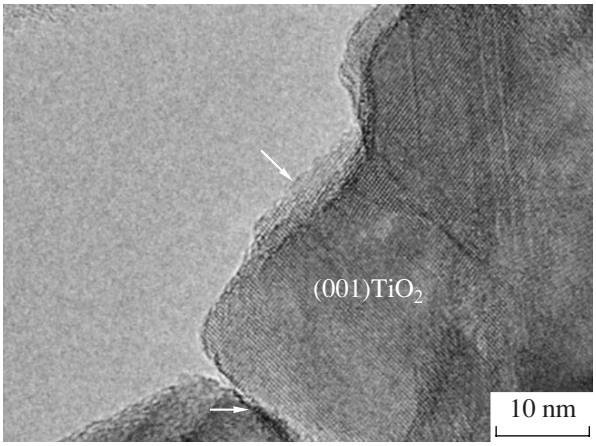

Fig. 4. Micrograph of an area of the Ce–Ti–O sample containing 5% CeO_2. T_{calcin} = 850°C. No crystallites of the cerium oxide phase are observed.

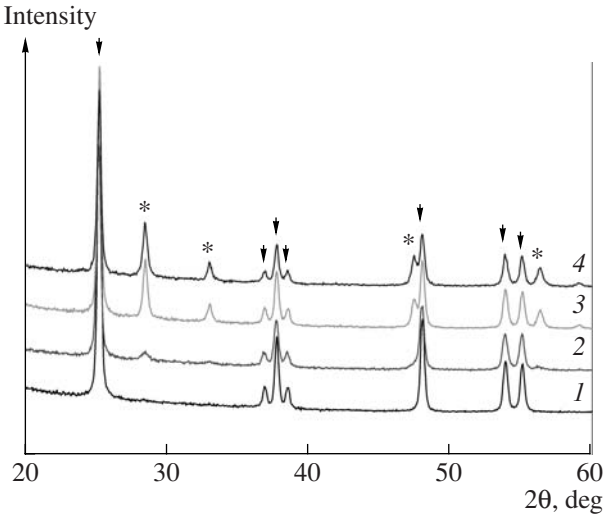

Fig. 5. X-ray diffraction patterns from the Ce–Ti–O samples containing (*1*) 3, (*2*) 5, (*3*) 10, and (*4*) 15 wt % CeO_2. T_{calcin} = 850°C. Reflection labeling: ↓, anatase; and *, CeO_2.

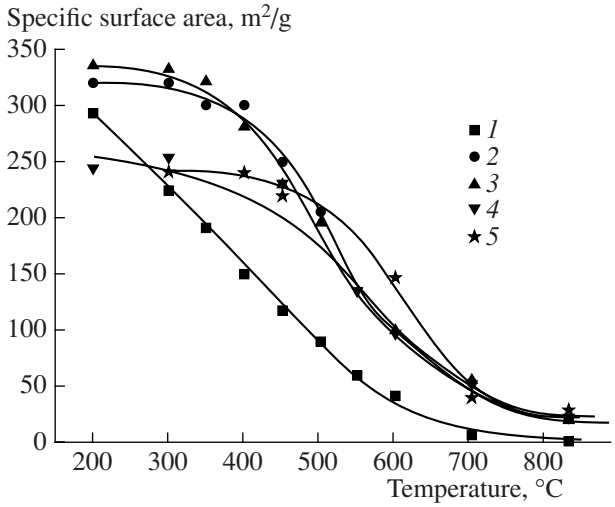

Fig. 6. Specific surface area as a function of the heat treatment temperature for (*1*) TiO_2 and (*2–5*) Ce–Ti–O materials with a CeO_2 content of (*2*) 3, (*3*) 5, (*4*) 10, and (*5*) 15 wt %.

phase are observed starting at 5 wt % CeO_2. Thus, anatase modified with cerium oxide is stable up to 850°C, while pure TiO_2 turns into rutile starting at 750°C.

The doping of titanium dioxide with cerium oxide not only modifies the phase composition of the former but also exerts a considerable effect on its porous structure (Table 2). Figure 6 plots the specific surface area of Ce–Ti–O materials and pure TiO_2 as a function of calcination temperature. The specific surface area of pure titanium dioxide decreases sharply with increasing temperature. Generally, titanium dioxide modified with cerium is thermally more stable than pure TiO_2. At a cerium oxide content of 3–5 wt %, the large specific surface area of the material (~300 m^2/g) persists up to a calcination temperature of 300–400°C and decreases as the temperature is further raised. The samples containing 10–15 wt % CeO_2 have a smaller specific surface area of ~250 m^2/g. In the temperature range 300–400°C, this effect is due to the higher extent of dispersion of anatase in the samples containing 3–5 wt % CeO_2. Particle sizing by the adsorption method demonstrated that the lower the cerium oxide content, the smaller the particle size of the sample. For example, the particle size is ~5.3 and 6.5–7.8 nm in the samples containing 3–5 and 10–15 wt % CeO_2, respectively. At the same time, the CSD domain size of anatase in these samples is the same.

As the calcination temperature is raised above 400°C, particle growth takes place (according to adsorption data) and the CSD size of anatase gradually increases (Table 2). From the fact that the particle size derived from adsorption data is somewhat larger than

Table 2. Texture parameters of Ce–Ti–O samples containing various amounts of CeO_2

Sample	T, °C	ρ, g/cm^3	S, m^2/g	V_s, cm^3/g	D_{dom}, nm	V_Σ, cm^3/g	ε, cm^3/cm^3	d_{CSD}, nm	d_{ads}, nm
3 wt % CeO_2	350	3.44	328	0.271	2.5	0.67	0.70	–	5.3
	400	3.48	329	0.266	3.1	0.68	0.70	–	5.2
	500	3.65	–	0.252	3.7	0.68	0.71	–	–
	600	–	93	–	–	–	–	13.0	16.4
	700	4.45	–	–	–	0.68	0.75	–	–
5 wt % CeO_2	300	3.51	323	0.320	2.6	0.67	0.70	5.0	5.3
	350	3.59	317	0.316	3.2	0.77	0.73	5.9	5.3
	400	3.52	276	0.311	3.1	0.67	0.70	6.0	6.2
	450	–	230	–	2.9	–	–	–	7.3
	500	3.62	196	0.323	3.9	0.66	0.70	7.2	8.5
	600	–	100	–	–	–	–	9.3	13.5
	740	4.43	50	–	–	0.68	0.75	–	27.1
10 wt % CeO_2	350	3.83	250	0.239	3.3	0.78	0.75	–	6.3
	450	3.92	228	0.258	3.2	0.79	0.75	–	6.7
	500	3.95	185	0.288	3.1	0.71	0.74	–	8.2
	550	4.01	135	0.237	3.1	0.69	0.73	–	11.1
	600	3.99	118	–	–	0.61	0.71	7.5	12.7
	700	3.97	53	0.192	7.1	0.62	0.71	–	28.5
15 wt % CeO_2	350	3.64	210	0.251	3.1	0.69	0.72	–	7.8
	500	3.67	160	0.244	3.1	0.66	0.71	–	10.2
	600	–	135	–	–	–	–	7.0	11.0
	700	4.10	36	0.218	11.5	0.61	0.70	–	40.6
	830	–	25	0.187	11.8	0.58	0.69	–	58.2

the CSD size of anatase, it can be inferred that anatase particles are sintered incoherently. Therefore, the decrease in the specific surface area of the materials at high temperatures is mainly due to the sintering of anatase particles.

Note that, up to 650°C, the higher the cerium oxide content of the cerium–titanium oxide sample, the less sharp the decrease in the specific surface area. For example, for the samples calcined at 600°C, the specific surface area increases with increasing cerium oxide content (Table 2). This is due to the decreasing mean particle size (d_{ads}) and the decreasing CSD size of anatase.

Both the pore volume and the porosity of the Ce–Ti–O materials (Table 2) show complicated, composition-dependent trends. The limiting sorption volume V_s, which is equal to the mesopore volume in the absence of micropores, is ~0.4 of the total pore volume V_Σ over the calcination temperature range of 300–500°C. As the temperature is further raised, the V_s/V_Σ ratio generally decreases. This is evidence that the total pore space of the materials is dominated by macropores. At the same time, the specific surface area of the materials is large owing to the mesoporous component of the texture. The variation of the mesopore volume between 350 and 500°C depends on the sample composition: this parameter decreases with increasing temperature for the sample containing 3 wt % CeO_2, is almost invariable for the sample containing 5 wt % CeO_2, and increases slightly for the other samples. The way the total porosity ε varies with the heat-treatment temperature is also composition-dependent. For the xerogels containing 3–5 wt % CeO_2, ε does not change noticeably; for the other samples, ε decreases.

Figures 7 and 8 plot the mesopore volume distribution over pore diameter for the Ce–Ti–O samples calcined at 350 and 500°C. Raising the CeO_2 content causes an increase in the dominant pore size D_{dom} in the first case and some decrease in D_{dom} in the second case. For the sample containing 3 wt % CeO_2, as the heat treatment temperature is raised, D_{dom} increases and the texture remains uniformly porous. Similar behaviors are shown by the samples containing 5 wt % CeO_2. By contrast, in the samples with a higher cerium oxide content, the initial D_{dom} value persists up to 500–550°C and then begins to increase.

This can clearly be seen from Figs. 9 and 10, which plot the pore volume distribution over pore diameter for the samples containing 5 and 10 wt % CeO_2. The mean pore diameter is 2.5–3 nm and is affected only slightly

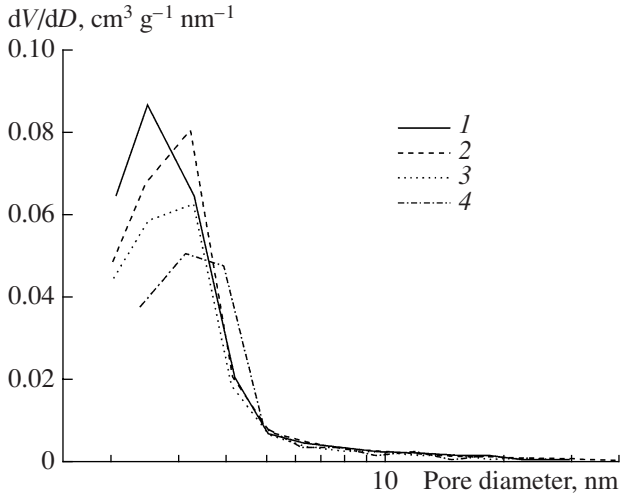

Fig. 7. Pore volume distribution over pore diameter for the Ce–Ti–O materials calcined at 350°C. CeO_2 content: (*1*) 3, (*2*) 5, (*3*) 10, and (*4*) 15 wt %.

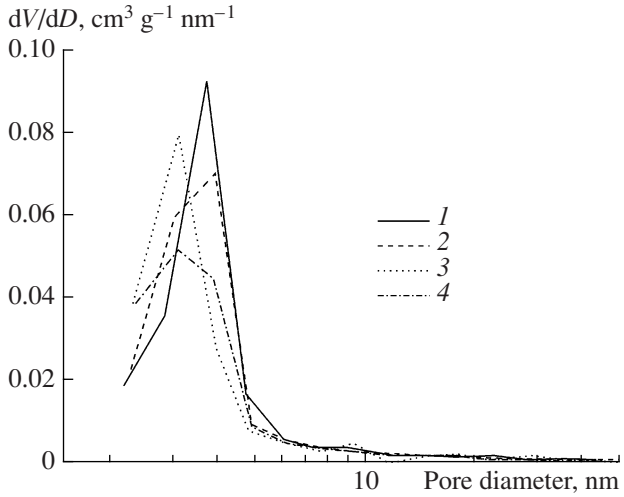

Fig. 8. Pore volume distribution over pore diameter for the Ce–Ti–O materials calcined at 500°C. CeO_2 content: (*1*) 3, (*2*) 5, (*3*) 10, and (*4*) 15 wt %.

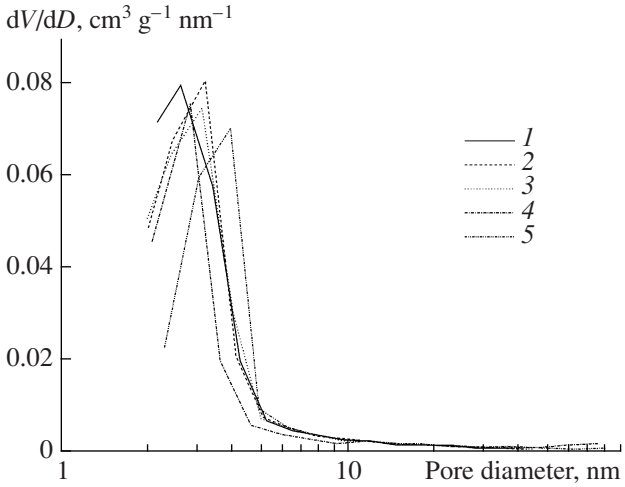

Fig. 9. Pore volume distribution over pore diameter for the 5 wt % CeO_2 + 95 wt % TiO_2 sample calcined at (*1*) 300, (*2*) 350, (*3*) 400, (*4*) 450, and (*5*) 500°C.

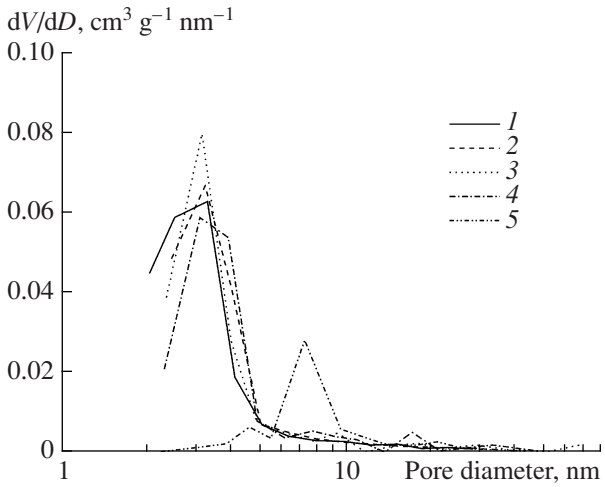

Fig. 10. Pore volume distribution over pore diameter for the 10 wt % CeO_2 + 90 wt % TiO_2 sample calcined at (*1*) 350, (*2*) 450, (*3*) 500, (*4*) 550, and (*5*) 700°C.

by calcination in the temperature range of 300–450°C. Raising the calcination temperature to 500–700°C causes a gradual increase in the pore size.

The above experimental data suggest that the formation of the structure of the Ce–Ti–O materials in the temperature range examined depends on the modifier content and proceeds in different ways in the samples containing 3–5 and 10–15 wt % CeO_2.

Sintering is among the main texture-transforming processes occurring during the high-temperature treatment of the xerogels. The detailed mechanism of sintering at a given temperature depends on the properties of the material, its chemical and phase compositions, and the environment. The sintering mechanism is deduced from the overall changes in pore structure parameters (porosity, specific surface area, and dominant pore size) [29]. At the same time, it is necessary to take into account the effect of the heat-induced phase transformation in the xerogel on the structure parameters.

For the Ce–Ti–O samples containing 3–5 wt % CeO_2, the heat-induced textural changes at 350–550°C, namely, the decrease in the specific surface area, the constancy of porosity, and the increase in the dominant pore size, indicate that sintering proceeds mainly by the surface diffusion mechanism. For the other samples, the bulk viscous flow mechanism comes into play, as is indicated by the decrease in the specific surface area, the decrease in porosity, and the approximate constancy of the dominant pore size. The thermodynamic analysis of the transfer of low-molecular-weight substances for

the basic high-temperature sintering mechanisms responsible for the textural changes is described in, e.g., [30].

Thus, the modification of titanium dioxide (anatase) with cerium oxide changes the properties of the initial material through the formation of nanostructured anatase Ce–Ti–O compounds that consist of incoherently intergrown fine TiO_2 crystallites and are separated by interblock (intercrystallite) boundaries stabilizing cerium ions. This stabilization is possible owing to the fact that the TiO_2 crystal structure at the interblock boundaries is disordered. The nanostructure formed in the Ce–TiO_2 system stabilizes the anatase phase, prevents the anatase particles from sintering at high temperatures, and allows modified anatase to retain a larger specific surface area and a higher porosity upon heat treatment than pure titanium dioxide does. The Ce–Ti–O samples containing 3–5 wt % CeO_2 are single phases up to 700°C, while traces of finely dispersed cerium oxide appear in the sample with a higher CeO_2 content. Above 800°C, rather large CeO_2 crystals are observed in all samples containing more than 3 wt % CeO_2. The sintering of the Ce–Ti–O xerogels between 350 and 550°C proceeds mainly via the surface diffusion mechanism for 3–5 wt % CeO_2 and via the bulk viscous flow mechanism for 10–15 wt % CeO_2.

REFERENCES

1. Nicolov, V., Klissurski, D., and Anastasov, A., *Catal. Rev. Sci. Eng.*, 1991, vol. 31, nos. 3–4, p. 319.
2. Cavani, P., Cavani, F., Manenti, J., and Trifiro, F., *Catal. Today*, 1987, vol. 1, nos. 1–2, p. 245.
3. Al'kaeva, E.M., Andrushrevich, T.V., Zenkovets, G.A., Kryukova, G.N., and Tsybulya, S.V., *Catal. Today*, 2000, vol. 61, nos. 1–4, p. 249.
4. Tsai, S-J. and Cheng, S., *Catal. Today*, 1997, vol. 33, nos. 1–3, p. 227.
5. Vorontsov, A.V., Savinov, E.N., Barannik, G.B., Troitsky, V.N., and Parmon, V.N., *Catal. Today*, 1997, vol. 38, no. 5, p. 732.
6. Zenkovets, G.A., Volodin, A.M., Bedilo, A.A., Burgina, E.B., and Kryukova, G.N., *Kinet. Katal.*, 1997, vol. 33, no. 5, p. 732 [*Kinet. Catal.* (Engl. Transl.), vol. 33, no. 5, p. 669].
7. Zenkovets, G.A., Tsybulya, S.V., Burgina, E.B., and Kryukova, G.N., *Kinet. Katal.*, 1999, vol. 40, no. 4, p. 623 [*Kinet. Catal.* (Engl. Transl.), vol. 40, no. 4, p. 562].
8. Zenkovets, G.A., *Doctoral (Chem.) Dissertation*, Novosibirsk: Inst. of Catalysis, 2004.
9. Molchanov, V.V. and Buyanov, R.A., *Usp. Khim.*, 2000, vol. 69, no. 5, p. 476.
10. Zenkovets, G.A., Gavrilov, V.Yu., Kryukova, G.N., and Tsybulya, S.V., *Kinet. Katal.*, 1998, vol. 39, no. 1, p. 122 [*Kinet. Catal.* (Engl. Transl.), vol. 39, no. 1, p. 114].
11. Zenkovets, G.A., Gavrilov, V.Yu., Kryukova, G.N., Tsybulya, S.V., and Parmon, V.N., *Kinet. Katal.*, 2002, vol. 43, no. 4, p. 621 [*Kinet. Catal.* (Engl. Transl.), vol. 43, no. 4, p. 573].
12. Busca, G., Lietti, L., Ramis, G., and Derti, F., *Appl. Catal., B*, 1998, vol. 18, no. 1, p. 1.
13. Gavrilov, V.Yu., Zenkovets, G.A., Zalomaeva, O.V., and Tsybulya, S.V., *Kinet. Katal.*, 2004, vol. 45, no. 5, p. 742 [*Kinet. Catal.* (Engl. Transl.), vol. 45, no. 5, p. 702].
14. Larsson, P-O. and Andersson, A., *J. Catal.*, 1998, vol. 179, no. 1, p. 72.
15. Jiang, X., Lou, L., Chen, Y., and Xiaoming Zheng, *Catal. Lett.*, 2004, vol. 94, nos. 1–2, p. 49.
16. Dong Guoli, Wang, Jianguo, Gao, Yinben, and Chen Songyin, *Catal. Lett.*, 1999, vol. 58, no. 1, p. 37.
17. Pavasupree, S., Suzuki, Y., Pivsa-Art, S., and Yoshikava, S., *J. Solid State Chem.*, 2005, vol. 178, no. 1, p. 128.
18. Leonov, A.I., Piryutko, M.M., and Keler, E.K., *Izv. Akad. Nauk SSSR, Ser. Khim.*, 1966, no. 5, p. 787.
19. Bazuev, G.V., Makarova, Shch.V., Zhilyaev, V.A., and Shveikin, G.P., *Zh. Neorg. Khim.*, 1976, vol. 21, no. 10, p. 1967.
20. Kuskov, V.D., Zverlin, A.V., Zaslavskii, A.M., Melnikov, A.V., and Slivinskaya, A.V., *Zh. Neorg. Khim.*, 1991, vol. 36, no. 11, p. 2757.
21. Preuss, A. and Gruehn, R., *J. Solid State Chem.*, 1994, vol. 110, no. 2, p. 363.
22. Bazuev, G.V., Makarova, Shch.V., and Shveikin, G.P., *Zh. Neorg. Khim.*, 1978, vol. 23, no. 6, p. 1451.
23. Luo, M., Chen, J., Chen, L., Lu, J., Feng, Z., and Li, C., *Chem. Mater.*, 2001, vol. 13, p. 197.
24. Dausher, A., Wehrer, P., and Hilaire, L., *Catal. Lett.*, 1992, vol. 14, no. 2, p. 171.
25. Rynkowsky, J., Farbotko, J., Touroude, R., and Hilaire, L., *Appl. Catal., A*, 2000, vol. 203, no. 2, p. 335.
26. Barret, E.P., Joyner, L.G., and Hallenda, P.H., *J. Am. Chem. Soc.*, 1951, vol. 73, no. 1, p. 373.
27. Guinier, A., *Theorie et technique de la radiocristallographie*, Paris: Dunod, 1956.
28. Dobrovol'skii, I.P., *Khimiya i tekhnologiya oksidnykh soedinenii titana* (Chemistry and Production of Titanium Oxides), Sverdlovsk: Ural. Otd. Akad. Nauk SSSR, 1988.
29. Gavrilov, V.Yu., *Doctoral (Chem.) Dissertation*, Novosibirsk: Inst. of Catalysis, 1999.
30. Geguzin, Ya.E., *Fizika spekaniya* (Physics of Sintering), Moscow: Nauka, 1984.